Evaluation of the PG Method for Modeling Unsteady flows in Complex Bathymetries

Arturo S. Leon[a,*], Christopher Gifford-Miears[b]

[a] *Department of Civil and Environmental Engineering, University of Houston, Cullen College of Engineering Building 1, 4726 Calhoun Road, Room N107, Houston, TX 77204-4003, USA*
[b] *Montgomery Watson and Harza, 1560 Broadway, Suite 1800, Denver, CO 80202, USA*

Abstract

The performance graph (PG) hydraulic routing method has been shown to be accurate, numerically efficient, and robust for unsteady flow routing. However, up to present, the performance graphs are constructed using one-dimensional (1D) steady flow models only, which are often questioned when simulating flows through complex bathymetries. This paper investigates whether the PG method can still be used when utilizing two-dimensional (2D) models for the construction of PGs. The test case is a stretch around an island in the Fraser River in British Columbia. The results show that the PG method is still applicable when utilizing a 2D steady flow model. The results also show that once the PGs are constructed, the PG routing method (1D and 2D) is computationally more efficient than the unsteady HEC-RAS model and can be several orders of magnitude faster than TELEMAC-2D.

Keywords: Complex river bathymetry, Hydraulic routing, Numerical modeling, Performance graph, Unsteady flow, Two-dimensional modeling

---

1. Introduction

Optimization problems involving short-term reservoir operation or real-time flood control may require hundreds or thousands of simulations (e.g., hydraulic

*Corresponding author
Email address: aleon3@uh.edu (Arturo S. Leon)

routing) for each operational strategy ([1], [2], [3], [4], [5], [6], [7]). Depending on the operational time-scale, relevant hydraulic information throughout the system may be required at a time resolution of an hour, or less (i.e., short-term operation) [8]. For these relatively short operational time-scales, robust and computationally efficient hydraulic routing methods are necessary.

A standard method for modeling unsteady flows in rivers is the application of the Saint-Venant equations. The Saint-Venant equations are a set of non-linear, partial differential equations that describe one-dimensional, unsteady open-channel flows. The Saint-Venant equations consist of conservation of mass and momentum equations and can be written as Equations (1) and (2), respectively (e.g., [9]):

$$\frac{\partial A}{\partial t} + \frac{\partial Q}{\partial x} = 0 \tag{1}$$

$$\frac{1}{g}\frac{\partial V}{\partial t} + \frac{\partial}{\partial x}\left(\frac{V^2}{2g}\right) + cos\theta\frac{\partial h}{\partial x} + S_f - S_o = 0 \tag{2}$$

where x = the distance along the channel; t = time, V = cross-sectional velocity; g = acceleration due to gravity; h = flow depth normal to x; A = cross-sectional area; Q = discharge; θ = angle between the channel bed and horizontal plane; S_o = bed slope; S_f = friction slope. The five terms in the momentum equation, Eq. (2), [from left to right] represent the local and convective acceleration, pressure force, friction force, and gravity force, respectively.

Due to non-linear terms in the Saint-Venant equations (i.e. convective acceleration), no exact analytic solution exists, except for special cases. Numerical methods used to solve the one-dimensional Saint-Venant equations include the Method of Characteristics, finite-difference, finite-element, and finite-volume schemes ([10] and [11]). Classic methods for solving the Saint-Venant equations are also presented in [12], [13], and others. Despite the wide array of numerical methods available for solving the Saint-Venant equations, the computational burden and lack of robustness (e.g., instabilities) still poses a problem ([14], [15]).

In an effort to address the issues of robustness and computational burden when solving the Saint-Venant equations, there have been several studies and applications determining suitability of simplified versions of the full Saint-Venant equations, or also called the dynamic wave equation (e.g. [16], [17]). Common approximations of the dynamic wave equation for use in unsteady flow routing include quasi-steady dynamic wave, noninertia wave, and kinematic wave models. Each of the aforementioned models exclude terms of the momentum equation, Eq. (2), to reduce computational complexity. The quasi-steady dynamic wave approximation for example, includes all terms in the full dynamic wave equation, Eq. (2), except for the local acceleration (i.e., $\frac{\partial V}{\partial t}$). Details for selection criteria to determine applicability of each approximation to unsteady flow routing can be found in [18] and [17].

A relatively new method for hydraulic routing of unsteady, open-channel flows utilizes the theory of *hydraulic performance graphs* (HPGs) ([19], [20], [21], [9]). HPGs summarize the dynamic relationship between water depths, or stages, at the upstream and downstream ends of a channel reach for a range of specified discharges. Volumetric performance graphs (VPGs) summarize the corresponding channel reach volume for each HPG flow scenario ([22]). Each of the HPG curves is known as a hydraulic performance curve (HPC) while as each of the VPG curves is known as a volumetric performance curve (VPC). In the remaining of the paper, HPGs and VPGs are denoted in general as PGs (performance graphs). Once the PGs are constructed, which is done only once, the PGs can be used over and over again for hydraulic routing with different initial and boundary conditions.

Even though the PG approach has been shown to be accurate, numerically efficient and robust for unsteady flow routing, so far, the PG method has only utilized one-dimensional (1D) steady-flow models for the construction of HPCs and VPCs (e.g., [19], [20], [21], [9]). One dimensional models are often questioned when simulating flows through complex bathymetries ([23]). This paper investigates whether the PG hydraulic routing method can still be used when utilizing two-dimensional (2D) models for the construction of the performance graphs. For the PG routing method to be applicable, the resulting family of curves conforming the HPGs and VPGs need to be monotonic and they must not cross each other. This paper also compares the accuracy and numerical efficiency (CPU time) of the PG routing method and those of the unsteady HEC-RAS model and the unsteady TELEMAC-2D model. The paper is organized as follows: (1) the suitability of two-dimensional hydrodynamics models for the construction of PGs is assessed; (2) a brief overview of the PG hydraulic routing method is presented; (3) a brief overview of the HEC-RAS ([24]) and TELEMAC-2D models ([25], [26]) is presented; (4) the PG routing method (using a 1D and 2D steady flow model), the unsteady HEC-RAS and TELEMAC-2D models are applied to a stretch around an island in the Fraser River in British Columbia; and (5) the key findings are summarized in the conclusion.

2. Suitability of two-dimensional hydrodynamics models for the construction of PGs

The PG routing method is based on the one-dimensional steady gradually varied flow approximation of the Saint-Venant equation [20]. This is equivalent to the so-called quasi-steady dynamic wave approximation which for a near horizontal channel is given by (e.g., [20])

$$\frac{V}{g}\frac{\partial V}{\partial x} + \frac{\partial h}{\partial x} - (S_o - S_f) = 0, \tag{3}$$

Since the flow is steady, V and h are a function of x only and hence the partial derivatives in Equation (3) can be replaced with total derivatives. The resulting equation can be discretized as

$$\frac{1}{2g}\frac{\Delta V^2}{\Delta x} + \frac{\Delta h}{\Delta x} - \left(-\frac{\Delta z}{\Delta x} - \frac{h_f}{\Delta x} \right) = 0, \tag{4}$$

By eliminating Δx in Equation (4) and applying this equation between two consecutive sections 1 and 2 (1 is upstream of 2) gives

$$h_1 + \frac{U_1^2}{2g} + z_1 = h_2 + \frac{U_2^2}{2g} + z_2 + h_f \tag{5}$$

For flows in any dimension (e.g., two-dimensional), the energy equation in integral form for a control volume CV bounded by a control surface CS can be written as (e.g., [27])

$$\dot{Q}+\dot{W}_{shear} = \frac{\partial}{\partial t}\int \left(u+\frac{\left|\vec{U}^2\right|}{2}+gz\right)\rho dV+\int_{cs}\left(u+\frac{p}{\rho}+\frac{\left|\vec{U}^2\right|}{2}+gz\right)\rho\vec{U}\cdot\vec{n}dA, \tag{6}$$

where u is the internal energy, $\vec{U}^2/2$ is the kinetic energy and gz is the potential

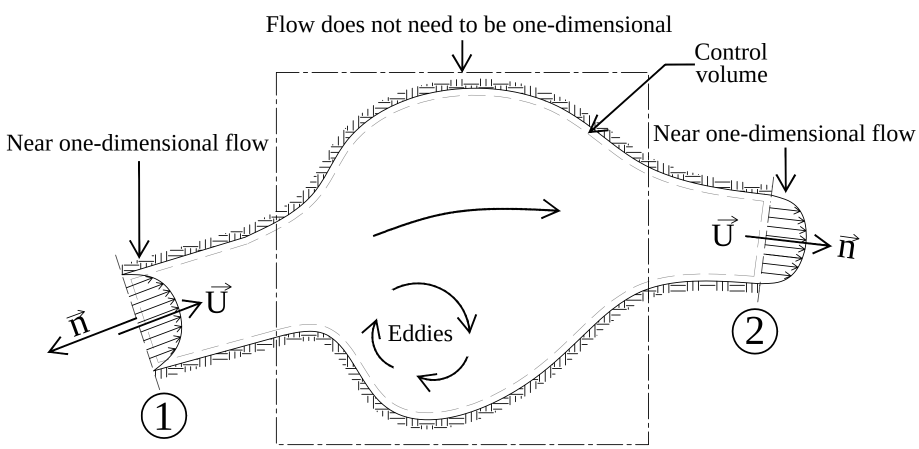

Figure 1. Control volume representation within a river reach; $\vec{n}$ and $\vec{U}$ represent the outward normal and velocity vectors, respectively

energy, p is pressure, ρ is density, g is the acceleration of gravity, A is area, n is the unit normal vector to the control surface, $\dot{Q}$ is the rate of heat added on system, $\dot{W}_{shear}$ is the shear work done on system. For a steady flow, the first term of the right hand side is zero. In addition, **for uniform flow properties at the inlet** (section 1) **and outlet** (section 2) [see Figure 1] with control sections normal to the local flow direction, Equation (6) can be reduced to (e.g., [27]):

$$\frac{p_1}{\rho_1} + \frac{\left|\vec{U}_1^2\right|}{2} + gz_1 = \frac{p_2}{\rho_2} + \frac{\left|\vec{U}_2^2\right|}{2} + gz_2 + \left[u_2 - u_1 - \frac{\dot{Q}}{\dot{m}} - \frac{\dot{W}_{shear}}{\dot{m}}\right] \tag{7}$$

where $\dot{m}$ is the mass flow rate. The term in square brackets in Equation (7) is the total head loss and hence, this equation can be written as (e.g., [27])

$$h_1 + \frac{U_1^2}{2g} + z_1 = h_2 + \frac{U_2^2}{2g} + z_2 + h_{loss} \tag{8}$$

which is the typical representation of the energy equation. Note in Equation (7) that **near uniform and one-dimensional flow properties need to be insured only at the inlet and outlet of the control volume** (e.g., ends of reaches). The reader can notice that Equations (5) and (8) are the same and hence it is expected that one and higher-order (e.g., two-dimensional) gradually varied flow models are suitable for constructing PGs.

3. Performance Graph (PG) Hydraulic Routing method

The PG hydraulic routing method used herein is the same as that presented in [9] that was formulated for a general river network, including dendritic and looped. Following the PG routing method is briefly described.

1. Definition of river network, where nodes and river reaches are defined. As mentioned in the previous section, the flow at the ends of each reach should be near uniform and one-dimensional. Because in the PG routing method, the flow discharge and water surface elevations are only available at the end of reaches, the reaches should be selected according to where data is needed and the desired resolution.
2. Computation of Performances Graphs. HPGs and VPGs are obtained for each channel reach for as many flows and downstream boundary conditions as necessary to cover the region of possible pairs of upstream and

downstream stages in the reach. Once the PGs are constructed, they are plotted to visually check that they are free of numerically induced errors. Numerical errors may result in the superposition of curves or in curves that display oscillatory patterns. For the curves that present apparent problems, the simulations must be repeated with more stringent criteria. These may require decreasing Δx (interpolation between cross-sections) and adjusting convergence parameters for the steady flow simulations. This initial screening of the PGs results in the elimination of the aforementioned oscillatory patterns and superposition of curves. For a detailed description on the construction of HPGs the reader is referred to [19].

3. Boundary conditions, which are defined at the most upstream and downstream ends of the river system. The boundaries may include an inflow hydrograph, a stage hydrograph or a rating curve.
4. Assembling and solving a non-linear system of equations, which is the final step of the hydraulic routing. The equations include the reaches' HPGs and VPGs, compatibility of water stages at junctions, continuity at junctions and the systems initial and boundary conditions. The HPGs and VPGs are accessed as look-up tables.

Given that the hydraulics (HPGs and VPGs) of each reach are pre-computed, the PG routing method results in a robust and computationally efficient tool for analyzing unsteady river flows. For further details about the PG routing method, the reader is referred to [9].

4. Brief Overview of Unsteady HEC-RAS and TELEMAC-2D Models

Two hydrodynamic models were used in the present work, namely the one-dimensional HEC-RAS model ([24]) and TELEMAC-2D ([25], [26]). These models are briefly described next.

4.1. Unsteady HEC-RAS Model

The unsteady HEC-RAS model solves the full one-dimensional Saint-Venant equations (Eqs. 1 and 2) using the four-point implicit finite difference scheme

([24]). Standard applications of this model include flood wave routing and flooding inundation studies.

4.2. TELEMAC-2D

The open source TELEMAC-2D solves the two-dimensional shallow water equations using the finite-element or finite-volume method and a computation mesh of triangular elements ([28], [26]). In the present work we have used the finite volume method. Various turbulence closure schemes are implemented in TELEMAC-2D. The extended $k-\epsilon$ turbulence model is used in this paper to represent turbulence production and dissipation ([26]). Standard applications of the TELEMAC-2D model include dam break and flood inundation studies.

5. Fraser River Application

The test case is the Fraser River, which is the largest river in British Columbia and the fifth largest in Canada. Fraser River is also the tenth longest river in Canada, flowing with a length of 1,375 kilometers. The Fraser River test section extends from 500 meters downstream of the Patullo Bridge in Vancouver, Canada, to approximately 6.5 kilometers upstream. As shown in Fig. (2), the river reach consists of a branching flow around an island with a guiding dike upstream of the island. The plan view of velocity field around the guiding dyke simulated with TELEMAC-2D is shown in Fig. (3)

5.1. Generation of HEC-RAS cross-sections and TELEMAC-2D Mesh

The PG assumption requires that the flow is near one-dimensional (e.g., no recirculation) at the upstream and downstream ends of all reaches (e.g. see Fig. 4). The flows inside the reach do not need to be one-dimensional. For this study, the Fraser River stretch was divided into 22 reaches as shown in Fig. (5). The subdivision of the system into reaches was performed according to [19]. These authors suggest to divide the system into reaches according to channel geometry (a reach should be more or less uniform), roughness (a reach should have a similar roughness), structures such as bridges or culverts (a new

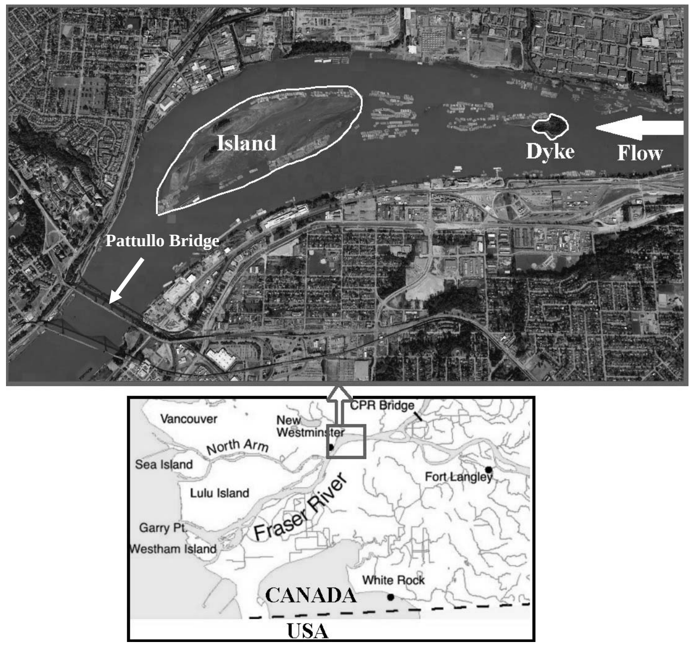

Figure 2. Fraser River test case: 6.5 Kilometer river section neighboring New Westminster, British Columbia

reach is placed at each side of the structure), and significant lateral flow from major sewers or tributaries (a reach should be added after significant inflow to the system). The geometric characteristics of the 22 reaches are shown in Table 1.

For the HEC-RAS model, the geometry was created using HEC-GeoRAS, a HEC-RAS extension to ArcGIS that acts as a pre- and post-processing tool to cut cross-sections from the Digital Terrain Model (DTM) provided by Northwest Hydraulic Consultants, Vancouver office. For the TELEMAC-2D model, an unstructured, triangular element mesh was generated to represent both the Fraser River domain mesh as well as the 22 individual PG reaches. Each mesh was generated by constrained Delaunay Triangulation using the freely available meshing tool, Blue Kenue, developed by the Canadian Hydraulics Centre of the National Research Council [29].

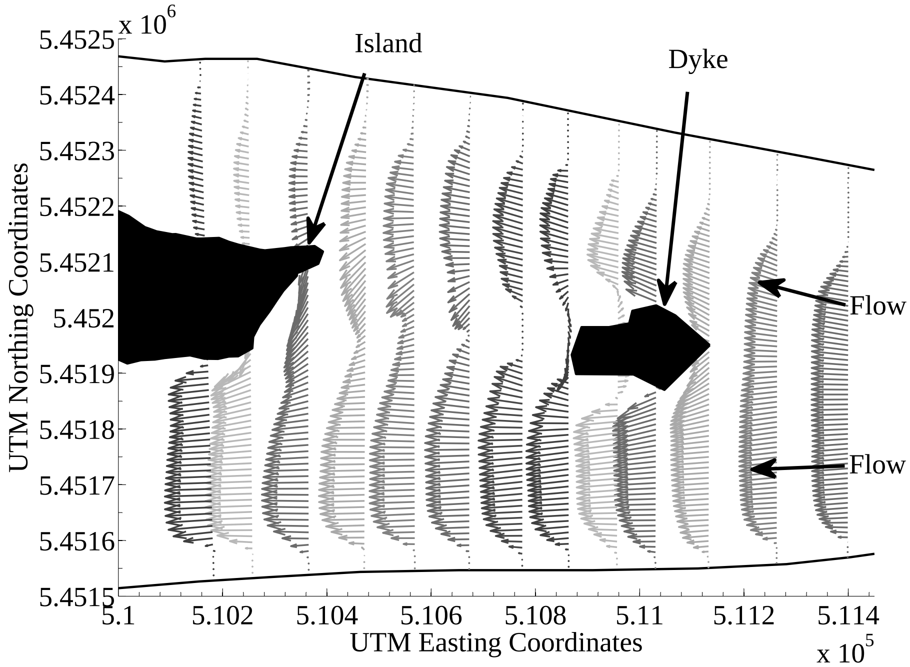

Figure 3. Plan view of velocity field around guiding dyke simulated with TELEMAC-2D

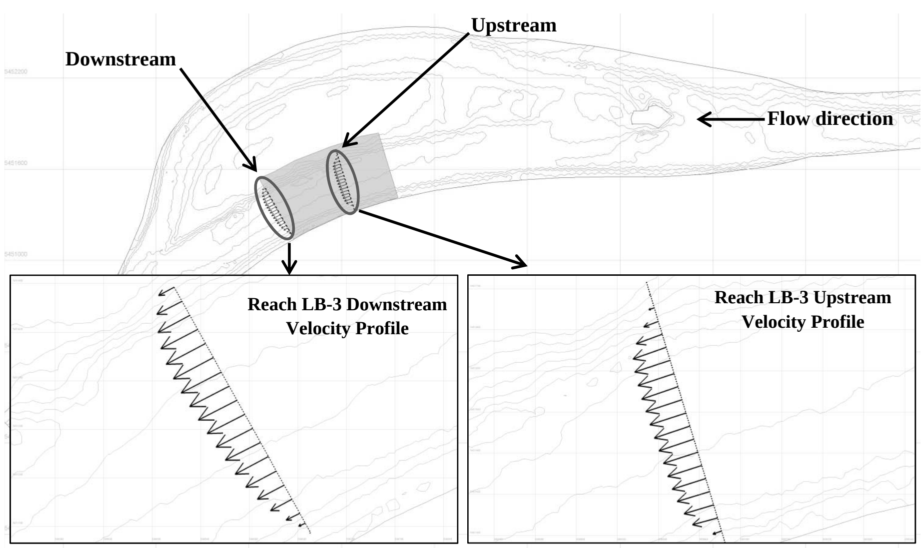

Figure 4. Reach depicting near one-dimensional flows at its upstream and downstream ends.

Table 1. Geometric characteristics of the reaches used in the test case

Reach ID	Upstream section	Downstream section	Length (m)	z_u (m)	z_d (m)
US-1	1	2	288.05	10.00	10.97
US-2	2	3	434.78	10.97	13.28
US-3	3	4	609.93	13.28	14.97
RB-0	4	5	274.33	14.97	13.99
RB-1	5	6	1582.08	13.99	20.08
RB-2	6	7	344.78	20.08	19.75
RB-3	7	8	478.21	19.75	16.65
RB-4	8	9	460.28	16.65	17.99
RB-5	9	10	343.74	17.99	17.73
RB-6	10	11	275.74	17.73	16.12
RB-7	11	12	304.40	16.12	16.00
RB-8	12	13	337.92	16.12	12.01
RB-9	13	14	137.24	12.01	9.77
LB-0	4	15	305.90	14.97	12.18
LB-1	15	16	1489.62	12.18	14.19
LB-2	16	17	506.62	14.16	12.03
LB-3	17	18	500.67	12.09	11.73
LB-4	18	19	562.02	11.73	13.81
LB-5	19	20	330.46	13.81	12.30
LB-6	20	14	156.72	12.30	9.77
DS-4	14	21	688.43	9.77	4.60
DS-5	21	22	570.00	4.60	12.30

5.2. Calibration of TELEMAC-2D

Calibration of the TELEMAC-2D model was performed using ADCP transect velocity data provided by Northwest Hydraulic Consultants (NHC), Vancouver office (British Columbia). Through this calibration, TELEMAC-2D was found to have a better agreement with the measured velocity data when using a Manning's roughness n of 0.04 $m^{1/3}$. Simulated (TELEMAC-2D) and measured velocity profiles for two transects are presented in Fig. (6). Due to lack of streamflow gages within the Fraser River study section, ADCP velocity measurements were the primary ground truth information available for calibration. A summary of the performance metrics (e.g., root mean square error, mean absolute error) comparing TELEMAC-2D results and the two ADCP velocity transects are shown in Table 2. Overall, the TELEMAC-2D model results com-

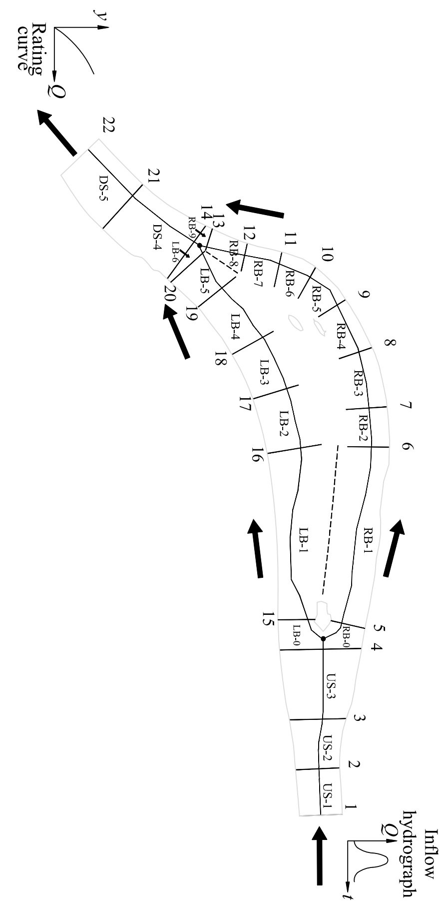

Figure 5. Reaches used for the Performance Graph routing

pare reasonably well with the two ADCP velocity transects. The Manning's roughness of 0.04 $m^{1/3}$ was also used for the HEC-RAS model.

To estimate the spatial discretization error and assess grid independence, the Grid Convergence Index (GCI) [30] method was used. The GCI is an index of the numerical uncertainty associated with a solution at a particular grid size, in comparison to another grid size, based on the Richardson extrapolation (RE) theory [31]. Application of Richardson extrapolation theory as a component of the GCI requires that the flow field be sufficiently smooth for the quantity of interest, convergence is monotonic, and that the numerical method is in its

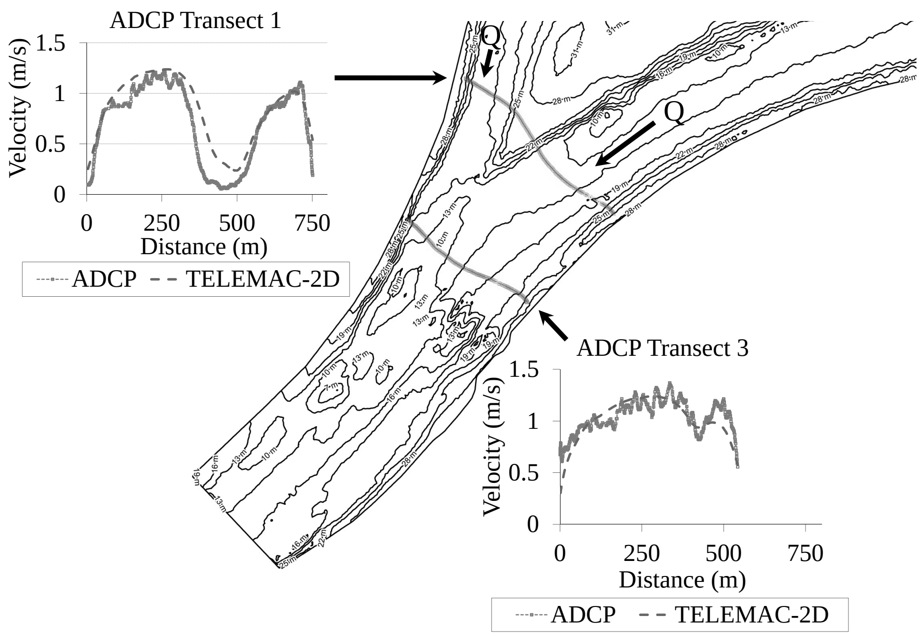

Figure 6. ADCP velocity transect measurements compared with results of TELEMAC-2D

asymptotic range [32]. The GCI procedure consists of five steps that systematically compare discrete solutions of a variable of interest, ϕ, between three or more grid resolutions, and estimate the discretization error multiplied by a factor of safety. A GCI value of zero would indicate that an exact solution has been achieved, which is not likely due to numerical and discretization errors. The Grid Convergence Index is calculated using the following equation ([31]):

$$GCI_{fine}^{21} = 1.25 \frac{e_a^{21}}{r_{21}^{p} - 1} \tag{9}$$

Where superscripts 1 and 2 represent the fine and coarse mesh resolution, e_a = relative error between solutions 1 and 2, and r_{21} = ratio of representative element sizes, and p = apparent order of accuracy. Using a factor of safety of 1.25 is akin to providing a 95% confidence interval for solutions of interest [31]. Grid resolutions tested were 5 m, 10 m, and 20 m element edge lengths using timesteps of 0.25, 0.50, and 1.00 second, respectively. Timestep sizes were chosen to maintain an approximately constant Courant number for each simulation. Grid resolutions and GCI values for variables of interest, WSE and Q, are shown in Tables 3 and 4, respectively.

Table 2. Performance metrics comparing TELEMAC-2D model results and the ADCP velocity transects shown in Fig. 6

Metric	TELEMAC-2D	
	Transect 1	Transect 3
Minimum residual (ft/s)	-0.59	-0.23
Maximum residual (ft/s)	0.11	0.48
Standard deviation (ft/s)	0.13	0.14
Root Mean Square Error (RMSE)	0.21	0.16
Mean Absolute Error (MAE)	0.0001	0.0007

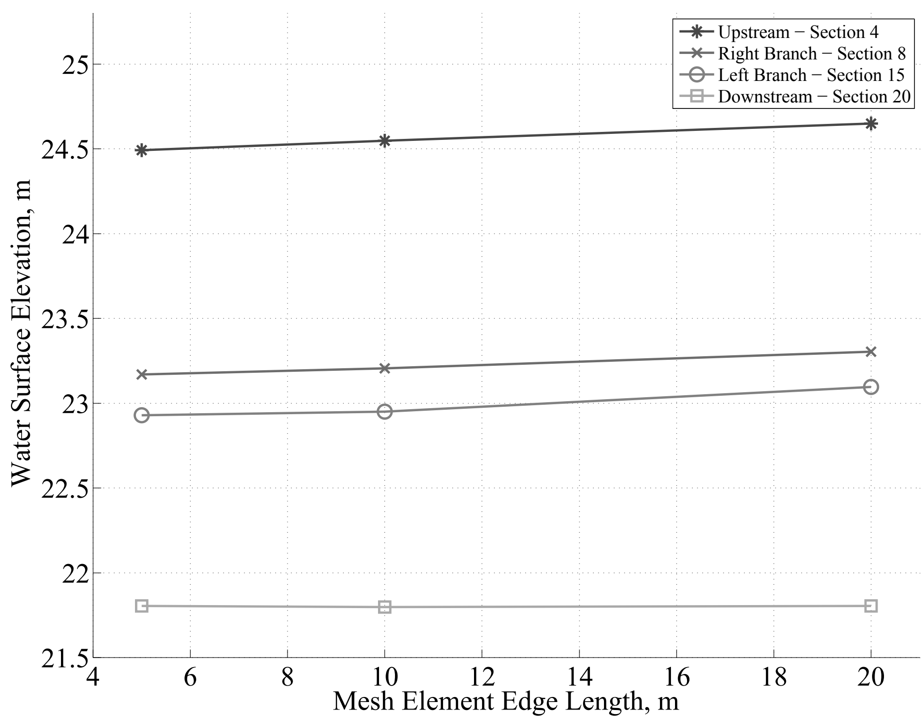

Figure 7. Averaged cross-sectional water surface elevation for three meshes at various cross-sections

According to Table 4, the numerical uncertainty on parameters of interest range from 0.1% to 1.51% for the finer grid (5 m) and 0.46% to 2.78% for the coarser grid (10 m). After comparing results for mesh element sizes of 5 m, 10

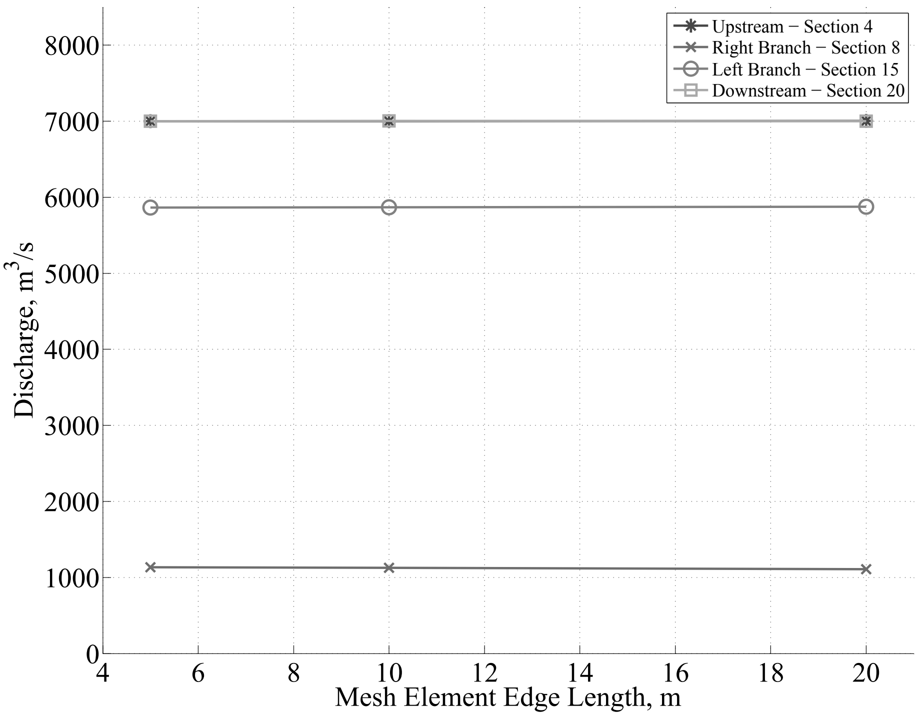

Figure 8. Flow discharge for three meshes at various cross-sections

m, and 20 m, it was determined that 10 m grid resolution was sufficient based on computational expense (e.g. each performance graph requires hundreds or thousands of simulations) and acceptable error for generation of performance graphs. The mesh convergence results for WSE and Q are shown in Figs. (7) and (8), respectively. These figures show that the water surface elevation and flow discharge are practically constant for the three meshes used, indicating that grid independence has been achieved.

Table 3. Mesh data used for the TELEMAC-2D Grid Convergence analysis

Mesh	Element size (m)	Δt (s)	Number of elements N
1	5	0.25	456962
2	10	0.50	114218
3	20	1.00	28379

A major benefit of the performance graph approach is the ability to remove

Table 4. Grid Convergence Index results

Reach	Location (See Fig. 5)	Variable	$GCI^{21}_{fine(5m)}$ (%)	$GCI^{32}_{coarse(10m)}$ (%)
Upstream	Section 4	Average WSE	1.512	2.781
		Discharge, Q	0.011	0.035
Right branch	Section 8	Average WSE	0.387	1.049
		Discharge, Q	1.174	2.152
Left branch	Section 15	Average WSE	0.071	0.460
		Discharge, Q	0.553	0.667

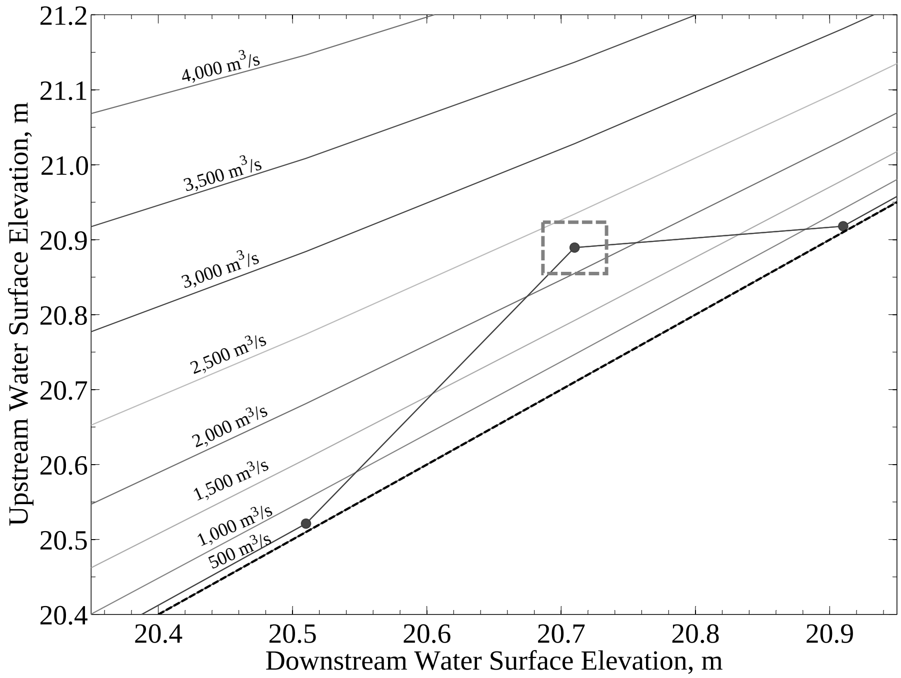

Figure 9. Example of instability problem for HPC at 500 m^3/s

instabilities that could occur during the construction of the performance graphs. Fig. (9) shows an example of an instability that was removed and re-simulated
235 with updated parameters.

5.3. Boundary Conditions for generation of PGs

For HEC-RAS and TELEMAC-2D, the upstream boundary condition for each individual reach was a specified discharge, while the downstream boundary was a specified water depth. For TELEMAC-2D, in an effort to minimize the effect of the upstream discharge boundary condition, the mesh domain of each PG reach was extended as illustrated in Fig. (10). The purpose of extending the computational domain is to allow for flow development at the location of interest, which is the upstream end of the original reach. This extension was not necessary for the HEC-RAS model.

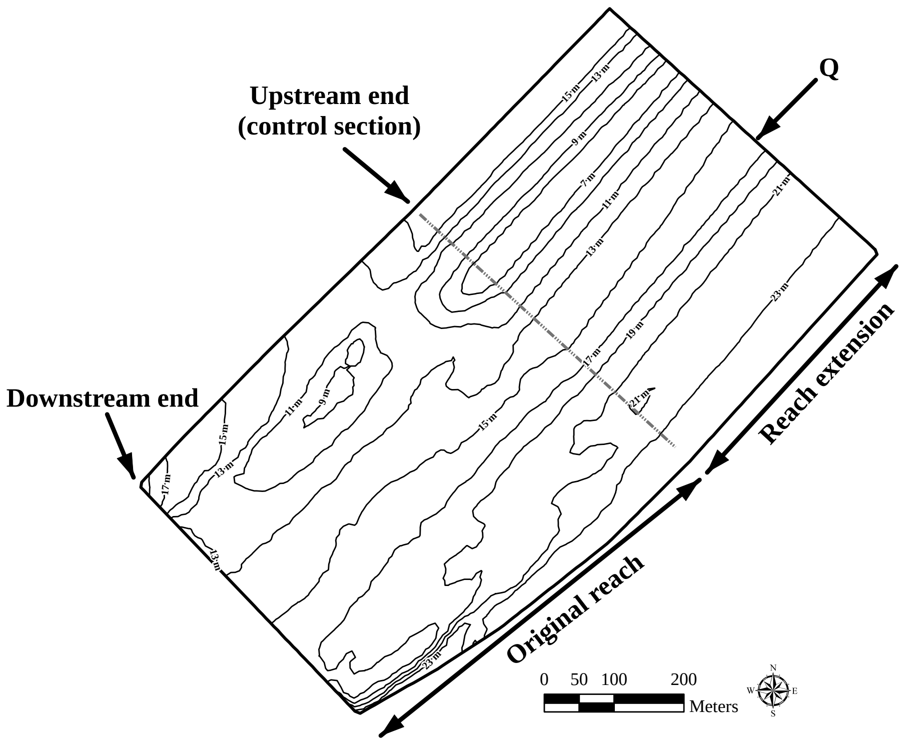

Figure 10. Reach extension at its upstream end when using TELEMAC-2D

5.4. Treatment of head losses at three-way junctions in the PG routing method

For approximating head-losses at junctions in the PG method, we project each nearest cross-section to the junction up to the approximate intersection of the reaches (junction) as an additional reach (e.g., Fig. 11). The additional reaches are treated as standard PG reaches. Then at the junction, the equation of continuity and water surface elevation compatibility condition are used. For more details see [9].

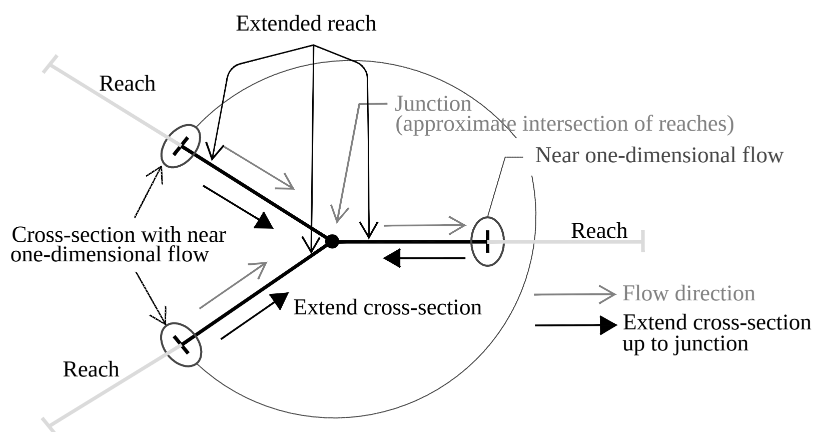

Figure 11. Schematic of treatment of head losses at three-way junctions for the PG routing method

5.5. Results

Generating PGs requires the computation of gradually varied flow scenarios for each reach (e.g., [19]). Each curve of the performance graph consists of a series of gradually varied flow (GVF) hydraulic simulations through a range of fixed downstream water stages, hence, each performance graph is composed of hundreds, potentially thousands of simulations dependent on desired resolution. The HEC-RAS and TELEMAC-2D simulations were conducted in a batch-style manner utilizing the Parallel Computing Toolbox within MATLAB and also using parallel batch scripts (e.g., [33]). Given that each hydraulic GVF simulation is solved independently of one another, embarrassingly parallel computation techniques can be employed (e.g. parametric sweeps, high performance computing clusters, etc.)

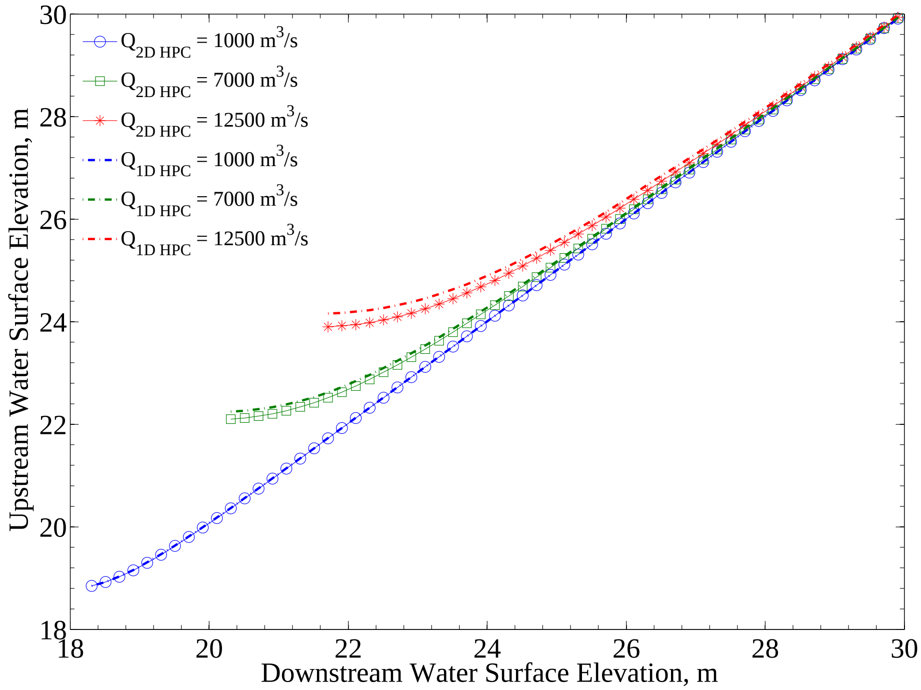

Figure 12. HPGs for reach US-3 generated with the steady HEC-RAS (1D) and steady TELEMAC-2D models

A comparison of HPGs and VPGs for reach US-3 generated with the steady TELEMAC-2D and steady HEC-RAS (1D) models are shown in Figs. (12) and (13), respectively. For displaying purposes, some of the HPCs and VPCs were removed intentionally. The relative difference in water depths between 1D and 2D HPCs is computed using Eq. (10).

$$\mathrm{E}_{h_{\text{2D-PG}}}(\%) = 100\left(\frac{h_{\text{2D-PG}} - h_{\text{1D-PG}}}{h_{\text{2D-PG}_{\max}} - h_{\text{2D-PG}_{\min}}}\right) \tag{10}$$

Each GVF simulation was performed using the same geometry and fixed downstream water surface elevations for both models. The relative difference in water depths are shown in Fig. (14). Results from Fig. (14) suggest that the individual HPCs yield a difference in computed depths of ± 0.1-4.0%, with discrepancies increasing as discharge rises. In general, the 1D HEC-RAS simula-

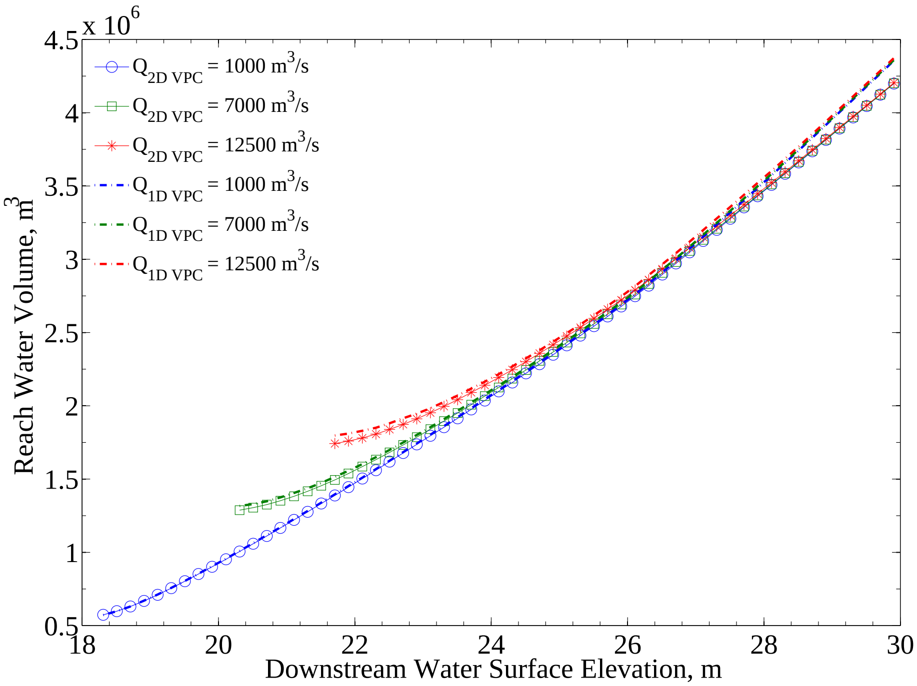

Figure 13. VPGs for reach US-3 generated with the steady HEC-RAS (1D) and steady TELEMAC-2D models

tions result in higher upstream water surface elevation (WSE) values suggesting that HEC-RAS predicted larger headlosses than TELEMAC-2D.

Performance graphs (HPGs and VPGs) using the steady HEC-RAS (1D) and steady TELEMAC-2D models were generated for all reaches and assembled as inputs for the PG routing. The PG routing method assembles and solves a nonlinear system of equations based on information summarized in the reaches HPGs and VPGs, continuity and compatibility of water stages at junctions, and the system's initial and boundary conditions [9]. Figure (15) shows outflow hydrographs obtained with the PG routing [constructed using the steady HEC-RAS (1D) and the steady TELEMAC-2D models], the unsteady TELEMAC-2D model and the unsteady HEC-RAS model. The comparison in Fig. (15) shows that similar results are obtained with these four models. The results also show that the 2D PG routing has a slightly better agreement with those

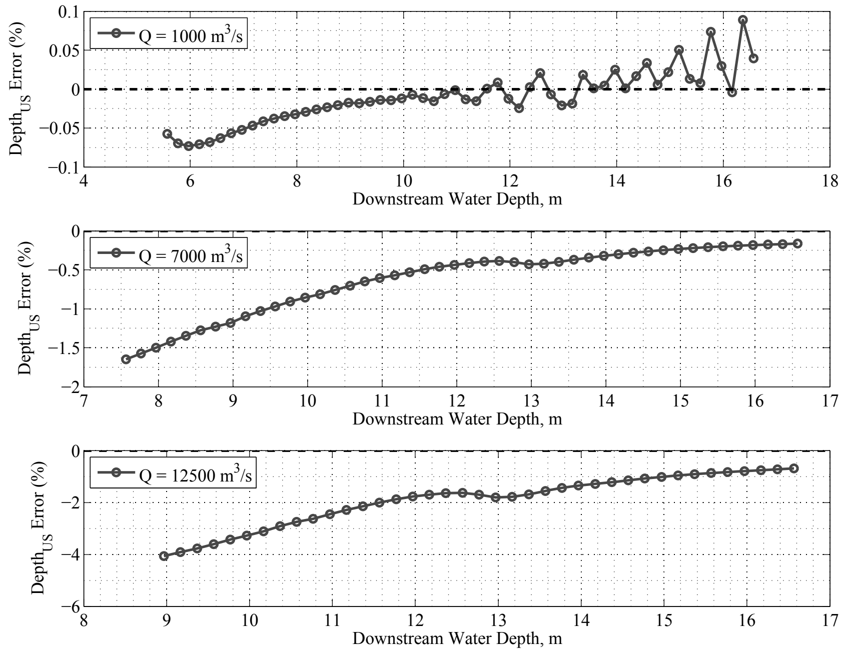

Figure 14. Relative difference in water depth between 1D and 2D HPCs for reach US-3

of the unsteady TELEMAC-2D model compared to the 1D PG routing. The previous results were expected because the 2D PG routing better quantifies the head losses compared to the 1D PG routing. The resulting CPU times for each model are shown in Table 5. Note that after the performance curves are constructed, the CPU time for the PG routing is independent of the model used for the generation of PGs. The CPU time calculation excluded the construction of the performance graphs for the PG routing method and the pre- and post-processing for the TELEMAC-2D and HEC-RAS models. The time step in the models is chosen such that the Courant number does not exceed one. In the TELEMAC-2D model case, the time step is relatively small because of the relatively small grid size. In the PG method, because the length of the reaches is much larger than the TELEMAC-2D grid size, the time step used in the PG method is also much larger than that used in the TELEMAC-2D model. As can be seen in Table 5, the computational efficiency of the PG routing (1D and 2D) is several orders of magnitude faster than TELEMAC-2D, and is significantly more efficient than the unsteady HEC-RAS model.

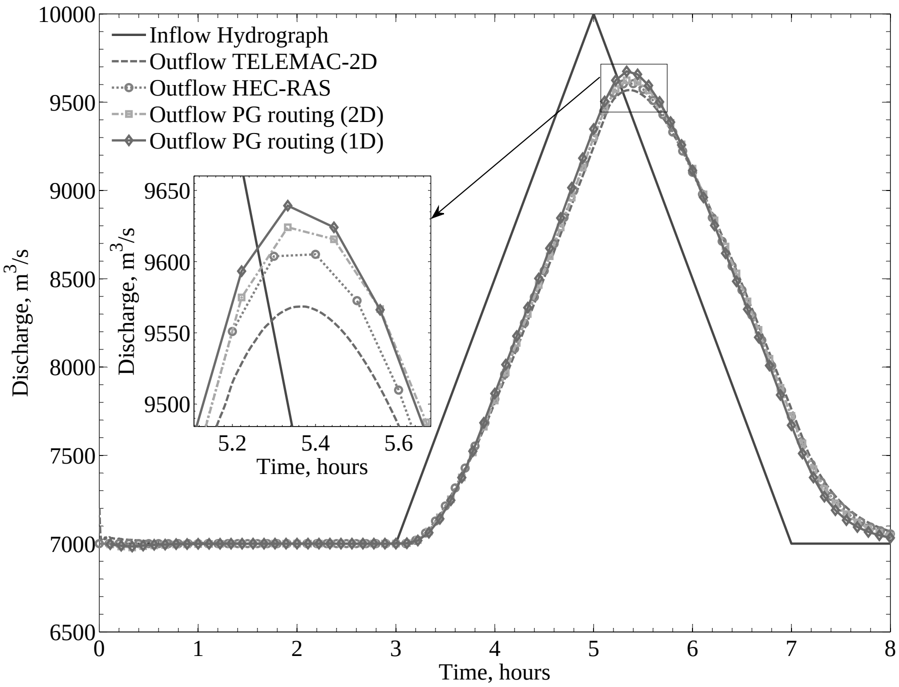

Figure 15. Outflow hydrographs obtained with the PG routing [constructed using the steady HEC-RAS (1D) and steady TELEMAC-2D models], the unsteady TELEMAC-2D model and the unsteady HEC-RAS model.

Table 5. Comparison of CPU times

Model	Δt (s)	CPU Time (s)
TELEMAC-2D	1.0	14,300
PG routing (1D and 2D)	400	0.56
HEC-RAS	360	5.41

6. Summary and Conclusions

This paper investigates whether the PG hydraulic routing method can still be used when utilizing two-dimensional (2D) models for the construction of the pre-computed performance curves (HPGs and VPGs). This paper also compares the accuracy and numerical efficiency (CPU time) of the PG routing and those of the unsteady HEC-RAS model and the unsteady TELEMAC-2D model. The test case is a stretch around an island in the Fraser River in British Columbia. The key findings are as follows:

1. The family of hydraulic performance curves produced using a steady 2D model are monotonic and don't cross each other. Thus, the PG routing method is still applicable when utilizing a 2D steady flow model for the construction of PGs.
2. In general, outflow hydrographs produced using the PG routing method (1D and 2D), the unsteady HEC-RAS model and the unsteady TELEMAC-2D models show very similar results.
3. The 2D PG routing has a slightly better agreement with those of the unsteady TELEMAC-2D model (assumed as the more accurate model of the four used) compared to the 1D PG routing. The previous results were expected because the 2D PG routing better quantifies the head losses compared to the 1D PG routing.
4. Once the HPGs and VPGs are constructed (regardless of the model used for their construction), the PG hydraulic routing method (1D and 2D) is computationally more efficient than the unsteady HEC-RAS model and can be several orders of magnitude faster than TELEMAC-2D.

   Overall, the PG routing (1D and 2D) is accurate, fast and robust and can be used even when simulating flows through complex river bathymetries. The 1D PG routing should be accurate enough for most applications, however if a more accurate quantification of head losses is necessary, the 2D PG routing can be used.

Acknowledgments

The authors gratefully acknowledge the financial support of the Bonneville Power Administration of the U.S. Department of Energy under award number

TIP#258. The authors would also like to thank Northwest Hydraulic Consultants (NHC), Vancouver, B.C., for providing the bathymetric data used for this study. Last but not least, we thank the editor and two anonymous reviewers for their constructive comments, which helped us to improve the manuscript.

References

[1] O. I. Unver, L. W. Mays, Model for real-time optimal flood control operation of a reservoir system, Journal Water Resources Management 4 (1) (1990) 21–46.

[2] M. Giuliani, S. Galelli, R. Soncini-Sessa, A dimensionality reduction approach for many-objective Markov Decision Processes: Application to a water reservoir operation problem, Environ. Model. Softw. 57 (2014) 101 – 114. doi:http://dx.doi.org/10.1016/j.envsoft.2014.02.011.

[3] A. S. Leon, E. Kanashiro, A new coupled optimization-hydraulic routing model for real-time operation of regulated river systems, in: Proc., Watershed Management Conference, Madison, WI, 2010, pp. 213–224.

[4] A. S. Leon, E. Kanashiro, T. Gichamo, R. Valverde, C. Gifford-Miears, Toward the intelligent control of river flooding, in: Proc., World Environmental and Water Resources Congress, Albuquerque, NM, 2012, pp. 1687–1696.

[5] A. S. Leon, E. Kanashiro, R. Valverde, V. Sridhar, Dynamic framework for intelligent control of river flooding: Case study, Journal of Water Resources Planning and Management 140 (2) (2014) 258–268. doi:10.1061/(ASCE)WR.1943-5452.0000260.

[6] T. Yang, X. Gao, S. L. Sellars, S. Sorooshian, Improving the multi-objective evolutionary optimization algorithm for hydropower reservoir operations in the California Oroville-Thermalito complex, Environ. Model. Softw. 69 (2015) 262 – 279. doi:http://dx.doi.org/10.1016/j.envsoft.2014.11.016.

[7] D. Chen, A. S. Leon, N. L. Gibson, P. Hosseini, Dimension reduction of decision variables for multireservoir operation: A spectral optimization model, Water Resources Research 52 (1) (2016) 36–51.

[8] S.-E. Fleten, T. K. Kristoffersen, Short-term hydropower production planning by stochastic programming, Computers & Operations Research 35 (8) (2008) 2656–2671.

[9] A. S. Leon, E. A. Kanashiro, J. González-Castro, Fast approach for unsteady flow routing in complex river networks based on performance graphs, Journal of Hydraulic Engineering 139 (3) (2013) 284–295.

[10] J. A. Cunge, F. M. Holly, A. Verwey, et al., Practical aspects of computational river hydraulics, Vol. 3, 1980.

[11] M. H. Chaudhry, Open-channel flow, 2nd Edition, Springer, 2008.

[12] K. Mahmood, V. M. Yevjevich, W. A. Miller, Unsteady flow in open channels, Vol. 1, Water Resources Publications Fort Collins, Colorado, USA, 1975.

[13] M. B. Abbott, Computational hydraulics: Elements of the theory of free surface flows, Pitman, London.

[14] A. S. Leon, N. Gibson, C. Gifford-Miears, Toward reduction of uncertainty in complex multireservoir river systems, The XIX International Conference on Computational Methods in Water Resources.

[15] N. L. Gibson, C. Gifford-Miears, A. S. Leon, V. S. Vasylkivska, Efficient computation of unsteady flow in complex river systems with uncertain inputs, International Journal of Computer Mathematics 91 (4) (2014) 781–797. doi:10.1080/00207160.2013.854336.

[16] F. Henderson, Open channel flow, Macmillan series in civil engineering, Macmillan, 1966.

[17] C. W. Tsai, Applicability of kinematic, noninertia, and quasi-steady dynamic wave models to unsteady flow routing, Journal of Hydraulic Engineering 129 (8) (2003) 613–627.

[18] V. M. Ponce, D. B. Simons, R.-M. Li, Applicability of kinematic and diffusion models, Journal of the Hydraulics Division 104 (3) (1978) 353–360.

[19] B. C. Yen, J. A. González-Castro, Open- channel capacity determination using hydraulic performance graph, *J. Hydraul. Eng.* 126 (2) (2000) 112–122.

[20] J. A. González-Castro, Applicability of the hydraulic performance graph for unsteady flow routing, Ph.D. thesis, Univ. of Illinois at Urbana-Champaign, Illinois. (2000).

[21] A. S. Leon, R. Valverde, J. Gonzalez-Castro, A Robust, Numerically Efficient Model for Unsteady Flow Routing in Topologically Complex River Networks, *Proc. World Environmental and Water Resources Congress* Albuquerque (2012) 1119–1128.

[22] M. A. Hoy, A. R. Schmidt, Unsteady flow routing in sewers using hydraulic and volumetric performance graphs, *Proc. World Environmental and Water Resources Congress* Nebraska (2006) 1–10.

[23] K. Marks, P. Bates, Integration of high-resolution topographic data with floodplain flow models, Hydrol. Process. 14 (2000) 2109–2122.

[24] Hydrologic Engineering Center, HEC-RAS, River Analysis System, Hydraulic Reference Manual. Version 4.1., U.S. Army Corps of Engineers, Davis, California., 2010.

[25] TELEMAC modelling system, TELEMAC-2D / User manual, TELEMAC modelling system (2010).

[26] J.-M. Hervouet, Hydrodynamics of free surface flows : modelling with the finite element method, John Wiley and Sons, Ltd, 2007.

[27] C. Kleinstreuer, Engineering fluid dynamics: an interdisciplinary systems approach, Cambridge Univ. Press, 1997.

[28] J. Galland, N. Goutal, J.-M. Hervouet, TELEMAC: A new numerical model for solving shallow water equations, *Advances in Water Resources* 14 (3) (1991) 138–148.

[29] Canadian Hydraulics Centre, Blue Kenue Reference Manual, Canadian Hydraulics Centre (2011).

[30] I. B. Celik, U. Ghia, P. J. Roache, et al., Procedure for estimation and reporting of uncertainty due to discretization in cfd applications, Journal of Fluids Engineering 130 (7).

[31] R. Hardy, S. Lane, R. Ferguson, D. Parsons, Assessing the credibility of a series of computational fluid dynamic simulations of open channel flow, Hydrological processes 17 (8) (2003) 1539–1560.

[32] H. K. Versteeg, An introduction to computational fluid dynamics the finite volume method, 2nd Edition, Pearson Education India, 2007.

[33] A. S. Leon, C. Goodell, Controlling HEC-RAS using MATLAB, Environmental Modelling & Software 84 (2016) 339 – 348.